

Intermittent Lagrangian velocities and accelerations in three-dimensional porous medium flow

M. Holzner, V.L. Morales, M. Willmann, and M. Dentz

This is the authors' final version of this article. Published version © 2015 American Physical Society, available from <http://dx.doi.org/10.1103/PhysRevE.92.013015>

Holzner, M., et al. 2015. Intermittent Lagrangian velocities and accelerations in three-dimensional porous medium flow. *Physical Review E: statistical, nonlinear, and soft matter physics*. 92(1): 013015. doi: 10.1103/PhysRevE.92.013015

Intermittent Lagrangian Velocities and Accelerations in Three-Dimensional Porous Medium Flow

M. Holzner* and M. Willmann
*Inst. of Environmental Engineering, ETH Zurich,
Wolfgang-Pauli-Str. 15, 8093 Zürich, Switzerland*

V.L. Morales
SIMBIOS Centre, University of Abertay, Bell Street Dundee DD1 1HG, Great Britain

M. Dentz
Spanish National Research Council (IDAEA-CSIC), c/Jordi Girona 18, 08034 Barcelona, Spain
(Dated: May 4, 2015)

Intermittency of Lagrangian velocity and acceleration is a key to understand transport in complex systems ranging from fluid turbulence to flow in porous media. High resolution optical particle tracking in a three-dimensional (3D) porous medium provides detailed 3D information on Lagrangian velocities and accelerations. We find sharp transitions close to pore throats, and low flow variability in the pore bodies, which gives rise to stretched exponential Lagrangian velocity and acceleration distributions characterized by a sharp peak at low velocity, superlinear evolution of particle dispersion and double peak behavior in the propagators. The velocity distribution is quantified in terms of pore geometry and flow connectivity, which forms the basis for a continuous time random walk model that sheds light on the observed Lagrangian flow and transport behaviors.

Intermittency of Lagrangian velocities and accelerations plays an important role in the understanding of transport in complex systems such as fluid turbulence [1–3], flow in porous media [4, 5], or animal locomotion [6, 7]. While in turbulence and animal motion, intermittency is caused by the characteristic spectrum of turbulent eddies and animal behavior, respectively, in porous media it arises due to the confined and complex pore space in which flow occurs. Continuum models of porous media [8] are based on the validity of the Darcy equation for fluid and Fick’s law for scalar fluxes on a representative elementary volume. Fluctuations of pore-scale flow and scalar transport are averaged out and represented in terms of effective parameters such as hydrodynamic dispersion. However, the intermittent behavior of pore-scale flow impacts on the nature of particle and scalar transport, and determines the way dissolved substances mix and react. The understanding of the origin of these processes is of both fundamental and practical importance in applications ranging from reactive transport in groundwater flow to diffusion in fuel cells or biological systems [9–11]. For engineered and natural porous media, they determine the mixing and dispersion of contaminants [12, 13], biofilm growth or the kinetics of chemical reactions [14–16]. On a fundamental level, pore-scale fluctuations may propagate to the continuum scale in a form that cannot be quantified by effective parameters [17], and give rise to non-Fickian transport behaviors [18, 19]. The qualitative and quantitative understanding of such collective phenomena requires the understanding of the physical origins of pore-scale flow fluctuations and intermittency. Advancements in experimental techniques have allowed for a leap in our understanding of transport in turbulent

flows by analysis of the Lagrangian properties of acceleration [20, 21]. However, analogous measurements in porous medium flow have been hindered by the difficulty of probing flow through a complex solid pore matrix in three dimensions, and at fine enough resolutions to detect intense gradients. Most optical experimental measurements, such as particle image velocimetry, provide Eulerian velocity information limited to one or two velocity components [22–26]. Nuclear magnetic resonance (NMR) measurements provide 3D flow information in real soil packings [15, 27, 28] and have measured a broad range of proton displacements. Recent work by Datta et al. [29] characterized the flow field from empirical Eulerian measurements to understand the spatial structure of the flow. Their findings present a correspondence between velocity fluctuations with the shape of the pore-space, which demonstrates that flow velocity is organized by the geometry of the porous medium. Statistics of velocity fluctuations from an Eulerian velocity field, however, cannot capture features of intermittency, which requires Lagrangian data instead. De Anna et al. [4] probed the flow through a 2D porous medium in greater detail by studying pore-scale flow simulations within a Lagrangian framework. Evaluation of fluid particle displacements revealed superdiffusive dispersion, while the analysis of Lagrangian velocities and accelerations displayed persistent zones of stagnation and correlations that decay quickly for acceleration but slowly for velocity. Despite its importance for pore-scale transport, mixing and reaction processes, little is known about intermittent flow organization with respect to the 3D pore-space geometry or the structural features of the porous medium that cause it.

In this work we employ an experimental 3D particle

tracking method that has been adapted to measure the flow velocity and accelerations along Lagrangian trajectories at high spatio-temporal resolution. Measurements are performed in a transparent porous medium that mimics the structure of sandy soil. Intermittent behavior of velocity and acceleration is observed and related to the succession of wide and narrow pore spaces along preferential flow channels. The strongest velocity and accelerations appear abruptly in the vicinity of pore throats, while in pore bodies the flow is nearly stagnant and velocities vary gradually. This double structure of the flow leads to anomalous transport as a consequence of the broad range of velocities and accelerations experienced by advected flow particles. To understand these behaviors, we develop a pore velocity model that accounts for pore geometry and connectivity and set up a continuous time random walk (CTRW) for the Lagrangian velocity and particle transitions.

Experimental set-up: We realize a transparent liquid saturated porous medium by filling a flow-through cell of dimensions $3.8 \times 3.8 \times 3.8 \text{ cm}^3$ with a mixture of two classes of Nafion grains of mean diameter $d_1 = 3.6 \text{ mm}$ and $d_2 = 0.5 \text{ mm}$, respectively, achieving a porosity of $\phi = 0.23$ (see supplementary material). Nafion granules have an irregular geometry resembling that of sand grains or pebbles similar to sand, and make up the porous material. Excellent matching of the index of refraction between solid phase and liquid is achieved with a 42 v/v % isopropanol aqueous solution (see supplementary material). The constant volumetric flow rate is 31.5 mL/min , the Darcy velocity is $q = 0.22 \text{ mm/s}$ and the average interstitial pore velocity is $v_p = q/\phi = 0.95 \text{ mm/s}$. The Reynolds number is $Re = qd_1/\nu \simeq 0.4$, well within the valid range for Darcy's law ($Re \leq 10$). An advective time scale can be defined as $t_A = d/v_p = 3.7 \text{ s}$. The liquid is seeded with neutrally buoyant fluorescent tracer particles with a diameter of $60 \mu\text{m}$ with a volume fraction concentration of 0.01%. The suspension is hence very dilute and hydrodynamic interactions between tracer particles are negligible. The Stokes number of the particles (defined as the ratio between particle response time $t_p = 2.7 \cdot 10^{-7} \text{ s}$ and advective time scale t_A) is $O(10^{-7})$, i.e., inertia effects are negligible. For the optical 3D particle tracking measurements we employ an Ar-Ion laser to illuminate the particles, a Photron high speed camera with a resolution of 1024×1024 pixels, operated at a framerate of 50 Hz and equipped with a four-way image splitter that mimics a multi-camera setup [30]. About 500 particles are tracked per frame for a duration of 4 min. Particle positions are determined with an accuracy of about $250 \mu\text{m}$ and trajectories are low-pass filtered to reduce position noise. Components of Lagrangian velocity u_i and accelerations a_i ($i = x, y, z$), as well as the components $\epsilon_{ij} = \partial u_i / \partial x_j$ of the Lagrangian deformation rate tensor and its symmetric part $s_{ij} = (\epsilon_{ij} + \epsilon_{ji})/2$, the rate of strain tensor, are computed [31, 32]. For spatial differen-

tiation all particles are considered assuming steady flow. The strain rate is denoted by $\mathcal{S} = \sqrt{\sum_{ij} s_{ij} s_{ij}}$. Average flow is along the positive x -direction, while y and z are the cross-sectional coordinates.

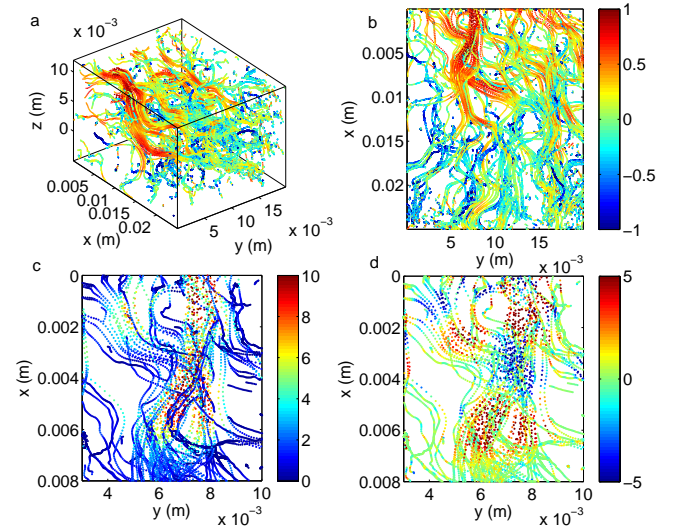


FIG. 1. Three- (a) and two-dimensional (b) views of the logarithm of the velocity magnitude $\ln(|\mathbf{u}|)$ normalized by its standard deviation along Lagrangian trajectories that are longer than 200 frames in a portion of the observation volume. Magnified views of the velocity u_x (c) and acceleration a_x components normalized by their standard deviations (d).

Experimental observations: Figs. 1a and b show the logarithm of the velocity magnitude $\ln(|\mathbf{u}|)$ along Lagrangian trajectories in a portion of the observation volume. It is apparent that preferential flow paths develop where the velocity is high next to regions where velocities are much lower. The two magnified views of a high activity region show the velocity u_x [Fig. 1c] and acceleration a_x [Fig. 1d] components normalized by their standard deviations σ_u and σ_a . It is illustrated how intense velocities are reached in narrow pore throats where the trajectories converge. Here, accelerations are strong and change sign in correspondence to the relative maxima of velocity.

The probability density functions (PDFs) of longitudinal and transverse velocity components normalized by their standard deviations σ are shown in Fig. 2a. While the PDF of velocity in turbulent flow is typically of Gaussian shape, our measurements show that flow in a porous medium produces velocity PDFs with strongly non-Gaussian tails. The longitudinal velocity component has a strong positive and a weaker negative tail related to the occurrence of reversed flow. The transverse velocity components are slightly skewed, which is presumably related to finite size effects or small anisotropic regions. We note that the velocity PDF can be represented by a stretched exponential model, consistent with simulations in stochastically generated geometries [33]. Velocity PDFs with broad tails but simple exponential decay

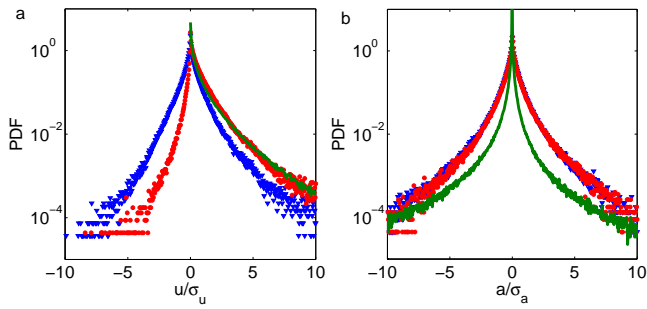


FIG. 2. PDFs of longitudinal (circles, red) and transverse (triangles, blue) Lagrangian velocity (a) and acceleration (b) components normalized by their standard deviations σ from experiment. Longitudinal velocity (a) and acceleration (b) from CTRW model (green line).

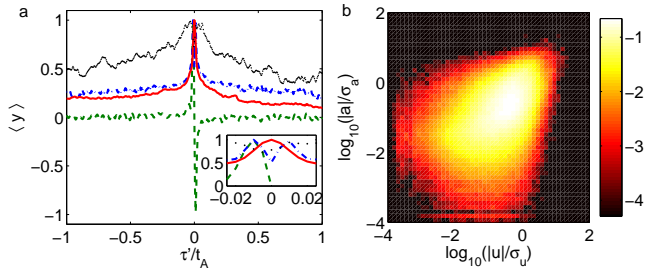


FIG. 3. (a) Conditionally averaged Lagrangian evolution of u_x (solid), a_x (dashed), $|a|$ (dash-dotted) and \mathcal{S} (dotted). The inset is a close-up at the origin. (b) Joint PDF of $|u_x|$ and $|a_x|$.

were observed in experiments in bead packs [27–29] and 2D simulations of a medium composed of disks [34].

Measurements of the distributions of accelerations are shown in Fig. 2b, which illustrates the PDFs of longitudinal and transverse accelerations normalized by their standard deviations σ_a . The PDFs of both acceleration components follow a stretched exponential shape and overlap, i.e., they do not show features of anisotropy. Their shape is similar to the one of the velocity PDF [Fig. 2a] and resembles typical acceleration PDFs in turbulent flow [20, 21]. This points to a possible universal character of the distribution of acceleration that is shared among different correlated fluid flows [20].

The intermittent and interdependent attributes of Lagrangian velocity and acceleration in porous medium flow can be understood qualitatively from Figs. 1c and d. Fast and strong acceleration events coincide with high velocities localized in pore throats, while acceleration events are weak in pore bodies characterized by almost stagnant velocities. As a consequence, Lagrangian velocities and accelerations, which are sampled equidistantly in time along the particle trajectories, display sharp peaks at low magnitudes [Fig. 2]. This interdependence can be illustrated more quantitatively by considering the conditional averages $\langle \mathcal{Y}(t') \rangle = \langle \mathcal{Y}(t' + t_m) \rangle$ for $\mathcal{Y} = u_x, a_x$,

$|a|$ and \mathcal{S} , where t_m is the time at which u_x assumes a global maximum along the measured trajectory, and the angular brackets denote the average over all particle trajectories. Both velocity and acceleration rise steeply and show sharp (double) peaks around $t' = 0$ [Fig. 3a]. The longitudinal acceleration component reaches a positive peak shortly before $t' = 0$, followed by a rapid change to a negative peak of similar magnitude shortly after. Accordingly, the acceleration magnitude shows a positive double peak around the origin [inset of Fig. 3a]. Since flow converges in front of pore throats, fluid elements are strongly stretched in longitudinal direction, which is manifested in the rise of the strain rate [Fig. 3a]. While a local minimum is observed at $t' = 0$ [inset of Fig. 3a], highest stretching is reached before the maximum velocity, which is qualitatively similar to laminar flow through an orifice. This shows that strong events of velocity and acceleration occur at pore throats where fluid elements are exposed to high strain.

The joint PDF of $|u_x|$ and $|a_x|$ shows that mid to high values have a moderate degree of pointwise correlation [Fig. 3b]. That is, when velocity is high also accelerations are moderate to high and particles accelerate and decelerate strongly. A correlation, albeit weaker, is still present at low values of velocity and acceleration (also visible in [Fig. 3a]). Low velocities are persistent and commonly exposed to low accelerations, but they feature a finite probability of moderate accelerations [Fig. 3b]. We find that this high variability of velocity and accelerations leads to anomalous dispersive behavior. Propagators of advected tracer particle locations are characterized by a strong stagnant peak present throughout the investigated time period, and a smaller secondary mobile peak that develops at time $t \geq 10$ s and moves at average flow speed [Fig. 4a]. We hence note that preasymptotic transport behavior and Fickian transport is not reached within an observation time of $O(10)t_A$ and distance of $O(10)d_1$. Analogous observations of non-Fickian transport have been made in complex pore structures using NMR [35] and, more recently, using numerical simulations [36]. The root mean square displacement of particles features a ballistic behavior initially, before it transitions towards a possible super-diffusive regime [Fig. 4c]. In the following we explore the quantification of these observations in terms of the pore geometry and flow structure. To this end we develop a model for the PDF of pore-velocities and set up a simple physically based correlated CTRW model [4, 5, 37].

Stretched exponential velocity PDF: Note that flow through a single pore can be approximated by a parabolic profile characteristic of Poiseuille flow through a pipe $v(r) = v_m (1 - r^2/r_p^2)$ with v_m the maximum velocity in the pore and r_p the pore radius. Sampling this profile uniformly in space gives rise to the flat velocity PDF $p_v(v|v_m) = v_m^{-1}$ for $0 \leq v \leq v_m$ for a given maximum velocity v_m . The unconditional PDF of pore-velocities

then is given by

$$p_v(v) = \int_v^\infty dv_m v_m^{-1} p_m(v_m), \quad (1)$$

where $p_m(v_m)$ is the PDF of maximum pore velocities to be determined in the following. We note that for an arrangement of parallel, non-interacting pores with variable radius, the maximum pore-velocity v_m is determined by the constant pressure drop and the pore-radius r_p such that $v_m \propto (r_p/r_0)^2$ with r_0 a characteristic pore radius. For a serial arrangement, v_m is determined by the constant total flux and the pore-radius such that $v_m \propto (r_p/r_0)^{-2}$. For a connected pore network, we conjecture the dependence of v_m on the pore radius according to the power-law

$$v_m = v_0 (r_p/r_0)^\alpha \quad -2 \leq \alpha \leq 2 \quad (2)$$

with v_0 representing a characteristic pore velocity. The exponent α may be understood as a connectivity parameter that informs on the pore network geometry. As shown in Fig. 4d, the distribution of pore radii r_p can be well approximated by the exponential PDF $p_r(r_p) = \exp(-r_p/r_0)/r_0$. Combining the latter with (2) gives the stretched exponential PDF of maximum pore velocities, $p_m(v_m)$

$$p_m(v_m) = v_0^{-1} (v_m/v_0)^{1/\alpha-1} \exp\left[-(v_m/v_0)^{1/\alpha}\right]. \quad (3)$$

From (1), we then obtain the PDF of pore-velocities

$$p_v(v) = v_0^{-1} \Gamma[1 - \alpha, (v/v_0)^{1/\alpha}], \quad (4)$$

where $\Gamma(\alpha, v)$ is the the incomplete Gamma-function [38]. The characteristic velocity v_0 is given in terms of the mean pore velocity $\langle v \rangle = v_p$ as $v_0 = 2v_p/\Gamma(1 + \alpha)$. For small velocities $v \ll v_0$, $p_v(v)$ goes towards the constant $v_0^{-1}\Gamma(1-\alpha)$, for large $v \gg v_0$ it shows the stretched exponential behavior $p_v(v) \sim v_0^{-1} \exp[-(v/v_0)^{1/\alpha}]$. Notably, this velocity model explains the stretched exponential tail observed in the PDF of Lagrangian velocities in a series of pore-scale studies [33, 39] by the exponential distribution of pore radii and the connectivity exponent α in (2).

Continuous time random walk: The velocity PDF (4) is used in the framework of a CTRW model for particle displacements along the direction of the mean pressure gradient. This approach models particle movements as a random walk in space-time

$$x_{n+1} = x_n + \ell_n, \quad t_{n+1} = t_n + \tau_n. \quad (5)$$

The path segment of length ℓ follows the distribution of pore-length $p_\ell(\ell)$. The transition time τ_n between turning points is determined from the mean velocity along the segment $\bar{v}_n = (v_{n+1} + v_n)/2$ as $\tau_n = \ell/\bar{v}_n$. The velocities v_n at the turning points x_n of the CTRW are distributed

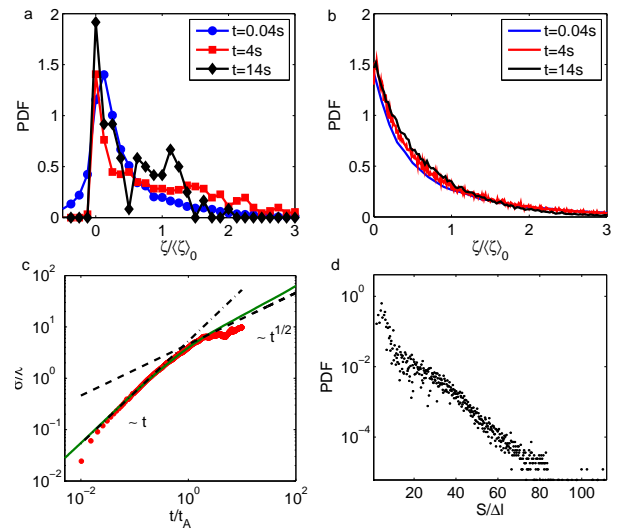


FIG. 4. PDF of propagators ζ of advected tracer particle locations at various displacement times in experiment (a) and model (b). $\langle \zeta \rangle_0 = v_p t$ is the expected nominal mean displacement. Root mean square displacement (c) and pore size PDF extracted from XRCT scan, voxel size $\Delta l = 50 \mu\text{m}$ (d).

according to $p_v(v)$ given by (4). Persistence of particle velocities in subsequent CTRW steps are modeled by a simple correlation model, which assigns a probability λ to stay at the same velocity or $1 - \lambda$ to change it at the turning point. Particle positions $x(t)$ at time t are given by linear interpolation of the positions at the turning points according to $x(t) = x_{n_t} + \bar{v}_{n_t}(t - t_{n_t})$, where n_t is the renewal process $n_t = \max(n | t_n \leq t)$. The longitudinal Lagrangian particle velocities then are given by $u_x = \bar{v}_{n_t}$. The average particle acceleration between turning points is measured by $a_n = (v_{n+1} - v_n)/\tau_n$. Accordingly, longitudinal particle accelerations are given by $a_x = a_{n_t}$. In the following, we set the connectivity parameter $\alpha = 3/2$ and $v_0 = 2v_p/\Gamma(1 + \alpha)$ to parameterize the velocity PDF (4). The distribution of pore-length is exponential with the characteristic length $\ell_0 = d/4$. The persistence of subsequent particle velocities is quantified by $\lambda = 9/10$.

This CTRW model quantifies quite well the PDF of Lagrangian velocities [Fig. 2a]. The peak at small velocities is captured by the CTRW in a natural way because particles spend more time in low velocity regions as quantified by the transition time $\tau_n = \ell/\bar{v}_n$. The acceleration PDF from CTRW captures the measured behavior qualitatively but not quantitatively [Fig. 2b]. We would not expect that the CTRW model posed above can resolve the acceleration PDF because it operates on a coarse scale (the scale of a pore), and cannot capture subpore velocity fluctuations. The particle propagators illustrated in Fig. 4a are qualitatively well described by the CTRW model [Fig. 4b]. The CTRW results are of the same order of magnitude and display a similar scaling behavior with $\langle \zeta \rangle_0$ as the experimental data. The

double peak behavior at late times cannot be captured by the present CTRW approach because it does not represent persistence of low and high velocity classes, which would be necessary to model such behavior. The evolution of particle dispersion is well captured by the CTRW model, both the ballistic short time behavior, as well as the onset of a possible super-diffusive regime [Fig. 4c].

In conclusion, our results show that flow in a soil-like porous medium is characterized by strongly intermittent velocity and acceleration. This establishes a connection between flow in porous media and turbulent flows which sheds new light on the understanding of the universal nature of complexity [40] in hierarchical flow systems. The experimental analysis elucidates the interdependence between Lagrangian velocity, acceleration and strain is experimentally probed to reveal a double structure of flow that localizes extreme events of low and high activity in the vicinity of pore throats and pore bodies. This double structure leads to anomalous dispersion, and produces non-Gaussian velocity and acceleration PDFs characterized by strong peaks in correspondence of the origin and stretched exponential tails. These features can be related to the pore-size distribution and flow connectivity, and are described by a CTRW model for the Lagrangian particle dynamics. These results shed light on the structure of Lagrangian dynamics in complex media and provide insight for the upscaling of transport from the pore to the continuum scale.

Acknowledgements: We acknowledge the contributions of R. Gallus and D. Sägger in the frame of a laboratory project, U. Gülan for help with data processing and W. Kinzelbach, T. LeBorgne, P. De Anna and P.K. Kang for stimulating discussions. Financial support is acknowledged from the Swiss National Science Foundation (SNF grant number 144645) for M.H., Marie Curie International Incoming Fellowships (FP7-PEOPLE-2012-SoilArchnAg) for V.L.M., and the European Research Council (ERC project MHetScale number 617511) for M.D.

* holzner@ifu.baug.ethz.ch

- [1] L. Biferale, G. Boffetta, A. Celani, B. Devenish, A. Lanotte, and F. Toschi, *Phys. Rev. Lett.* **93**, 064502 (2004).
- [2] R. Friedrich, J. Peinke, M. Sahimi, and M. Reza Rahimi Tabar, *Phys. Rep.* **506**, 87 (2011).
- [3] F. Toschi and E. Bodenschatz, *Annu. Rev. Fluid Mech.* **41**, 375 (2009).
- [4] P. De Anna, T. Le Borgne, M. Dentz, A. Tartakovsky, D. Bolster, and P. Davy, *Phys. Rev. Lett.* **110**, 184502 (2013).
- [5] T. Le Borgne, M. Dentz, and J. Carrera, *Phys. Rev. Lett.* **101**, 090601 (2008).
- [6] D. Kelley and N. Ouellette, *Sci. Rep.* , 3 (2013).
- [7] D. Kramer and R. McLaughlin, *Am. Zool.* **41**, 137 (2001).
- [8] J. Bear, *Dynamics of Fluids in Porous Media* (American Elsevier, New York, 1972).
- [9] A. Tartakovsky, D. Tartakovsky, and P. Meakin, *Phys. Rev. Lett.* **101** (2008).
- [10] I. Mankel *et al.*, *Appl. Phys. Lett.* **90**, 174105 (2007).
- [11] E. Codling, M. Plank, and S. Benhamou, *J. R. Soc. Interface* **5**, 813 (2008).
- [12] D. Lester, G. Metcalfe, and M. Trefry, *Phys. Rev. Lett.* **111**, 174101 (2013).
- [13] T. Le Borgne, M. Dentz, and E. Villermaux, *Phys. Rev. Lett.* **110**, 204501 (2013).
- [14] V. Morales, J.-Y. Parlange, and T. Steenhuis, *J. Hydrol.* **393**, 29 (2010).
- [15] J. Seymour, J. Gage, S. Codd, and R. Gerlach, *Phys. Rev. Lett.* **93**, 198103 (2004).
- [16] M. Dentz, T. Le Borgne, A. Englert, and B. Bijeljic, *J. Contam. Hydrol.* **120**, 1 (2011).
- [17] I. Battiato, D. Tartakovsky, A. Tartakovsky, and T. Scheibe, *Adv. Water Resour.* **32**, 1664 (2009).
- [18] J. P. Bouchaud and A. Georges, *Phys. Rep.* **195**, 127 (1990).
- [19] B. Berkowitz, A. Cortis, M. Dentz, and H. Scher, *Rev. Geophys.* **44**, RG2003 (2006).
- [20] A. La Porta, G. Voth, A. Crawford, J. Alexander, and E. Bodenschatz, *Nature* **409**, 1017 (2001).
- [21] N. Mordant, A. Crawford, and E. Bodenschatz, *Phys. Rev. Lett.* **93**, 214501 (2004).
- [22] S. Saleh, J. Thovert, and P. Adler, *AIChE J.* **39**, 1765 (1993).
- [23] A. Cenedese and P. Viotti, *Water Resour. Res.* **32**, 2329 (1996).
- [24] Y. Hassan and E. Dominguez-Ontiveros, *Nucl. Eng. Design* **238**, 3080 (2008).
- [25] A. Huang, M. Huang, H. Capart, and R.-H. Chen, *Exp. Fluids* **45**, 309 (2008).
- [26] D. Butscher, C. Hutter, S. Kuhn, and P. von Rohr, *Exp. Fluids* **53**, 1123 (2012).
- [27] Y. Kutsovsky, L. Scriven, H. Davis, and B. Hammer, *Phys. Fluids* **8**, 863 (1996).
- [28] L. Lebon, L. Oger, J. Leblond, J. Hulin, N. Martys, and L. Schwartz, *Phys. Fluids* **8**, 293 (1996).
- [29] S. Datta, H. Chiang, T. Ramakrishnan, and D. Weitz, *Phys. Rev. Lett.* **111**, 064501 (2013).
- [30] K. Hoyer *et al.*, *Exp. Fluids* **39**, 923 (2005).
- [31] B. Lüthi, A. Tsinober, and W. Kinzelbach, *J. Fluid Mech.* **528**, 87 (2005).
- [32] M. Holzner and B. Lüthi, *Phys. Rev. Lett.* **106**, 134503 (2011).
- [33] M. Siena, M. Riva, J. Hyman, C. Winter, and A. Guadagnini, *Phys. Rev. E* **89**, 013018 (2014).
- [34] A. Araújo, W. Bastos, J. Andrade, and H. Herrmann, *Phys. Rev. E* **74**, 010401 (2006).
- [35] U. Scheven, D. Verganelakis, R. Harris, M. Johns, and L. Gladden, *Phys. Fluids* **17**, 7107 (2005).
- [36] B. Bijeljic, A. Raeini, P. Mostaghimi, and M. Blunt, *Phys. Rev. E* **87**, 013011 (2013).
- [37] P. K. Kang, P. de Anna, J. P. Nunes, B. Bijeljic, M. Blunt, and R. Juanes, *Geophys. Res. Lett.* **41**, 6184 (2014).
- [38] M. Abramowitz and I. Stegun, *Handbook of Mathematical Functions* (Dover Publications, New York, 1972).
- [39] M. Moroni and J. Cushman, *Water Resour. Res.* **37**, 873 (2001).
- [40] N. Goldenfeld and L. P. Kadanoff, *Science* **284**, 87 (1999).